Available online at www.sciencedirect.com
SCIENCE DIRECT®
Comput. Methods Appl. Mech. Engrg. xxx (2004) xxx–xxx
Computer methods in applied mechanics and engineering
www.elsevier.com/locate/cma

Multiscale-stabilized solutions to one-dimensional systems of conservation laws

Ruben Juanes [a,*], Tadeusz W. Patzek [b,c]

[a] Department of Petroleum Engineering, Stanford University, 65 Green Earth Sciences Bldg., Stanford, CA 94305, United States
[b] Department of Civil and Environmental Engineering, University of California at Berkeley, 631 Davis Hall # 1710, Berkeley, CA 94720, United States
[c] Earth Sciences Division, Lawrence Berkeley National Lab, 1 Cyclotron Road Mailstop 90-1116, Berkeley, CA 94720, United States

Received 12 January 2004; received in revised form 15 July 2004; accepted 28 July 2004

Abstract

We present a variational multiscale formulation for the numerical solution of one-dimensional systems of conservation laws. The key idea of the proposed formulation, originally presented by Hughes [Comput. Methods Appl. Mech. Engrg., 127 (1995) 387–401], is a multiple-scale decomposition into resolved grid scales and unresolved subgrid scales. Incorporating the effect of the subgrid scales onto the coarse scale problem results in a finite element method with enhanced stability properties, capable of accurately representing the sharp features of the solution. In the formulation developed herein, the multiscale split is invoked prior to any linearization of the equations. Special attention is given to the choice of the matrix of stabilizing coefficients and the discontinuity-capturing diffusion. The methodology is applied to the one-dimensional simulation of three-phase flow in porous media, and the shallow water equations. These numerical simulations clearly show the potential and applicability of the formulation for solving highly nonlinear, nearly hyperbolic systems on very coarse grids. Application of the numerical formulation to multidimensional problems is presented in a forthcoming paper.

Keywords: Stabilized finite elements; Multiscale; Shock-capturing; Porous media flow; Shallow water equations

1. Introduction

Systems of conservation laws describe many physical processes of interest in science and engineering. Here, we consider nonlinear systems of the advection–diffusion type, for which the flux function may be

* Corresponding author.
E-mail address: ruben.juanes@stanford.edu (R. Juanes).

0045-7825/$ - see front matter © 2004 Elsevier B.V. All rights reserved.
doi:10.1016/j.cma.2004.07.026

split into a hyperbolic and a diffusive part. We are interested in the case of vanishing diffusion, for which the system becomes almost hyperbolic. In an attempt to obtain stable solutions which retain high-order accuracy, the equations are solved here using a stabilized finite element method, where the stabilizing terms arise naturally in a variational multiscale method [21,22]. The idea of a multiple-scale decomposition of the solution, which is now dominant in fluid mechanics, is adopted here for the simulation of multiphase porous media flow, and the shallow water equations. The oscillatory behavior of the classical Galerkin method is drastically reduced without compromising the computational cost of the method or the accuracy of the solution. The specific contributions of this paper may be succinctly summarized as follows:

1. Nonlinearity of the equations is retained at the time of invoking the multiscale split. Proper linearization of the stabilizing terms is introduced *after* the multiple-scale decomposition into resolved and unresolved scales. Furthermore, the multiple-scale solution is *not* reconstructed from point values of coarse and subgrid scales.
2. Several definitions of the matrix of stabilizing coefficients are tested and compared [10,23,40]. To reduce further or eliminate completely the localized oscillations that may persist in the stabilized solution, several existing shock-capturing techniques are studied [8,15,24,25,40], and a novel expression for the discontinuity-capturing diffusion is proposed.
3. The multiscale formalism is applied to the equations governing one-dimensional three-phase flow through porous media, extending previous work on miscible and immiscible two-phase flow [31,33].

The formulation presented here is quite different from other methods that account for multiple-scale phenomena, such as the multiscale finite element method [20], the subgrid upscaling technique [1,2], and the mortar upscaling method [39], where the main objective is to incorporate the small-scale heterogeneity. On the other hand, a recent paper [36] applies the original variational multiscale formulation of [21,22] to porous media flows. It is restricted, however, to the linear scalar equation describing steady-state, single-phase, Darcy flow, and the objective is to remove velocity–pressure instabilities, rather than instabilities arising from the nearly hyperbolic character of the equations.

In Section 2 we present the initial and boundary value problem. We give the weak form of the problem and describe the multiple-scale approach. Special attention is given to the matrix of stabilizing coefficients and to various shock-capturing techniques. In Section 3 we apply the formulation to three-phase flow in porous media. The first application is an oil filtration problem in a relatively dry medium, and the second reproduces water–gas injection in a hydrocarbon reservoir. Numerical solutions are compared with a general, newly developed, analytical solution [32]. In Section 4 we present the application of the method to the one-dimensional shallow water equations in conservation variables. These simulations illustrate the excellent performance of the proposed methodology. In Section 5 we gather the main conclusions, and anticipate ongoing and future research.

2. Multiscale numerical formulation

2.1. Initial and boundary value problem

The mathematical problem is defined (in dimensionless form) by the one-dimensional system of conservation laws

$$\partial_t \boldsymbol{u} + \partial_x(\boldsymbol{f}(\boldsymbol{u}) - \mathbf{D}(\boldsymbol{u})\partial_x \boldsymbol{u}) = 0, \quad x \in \Omega \equiv (0,1), \;\; t \in (0,T]. \tag{1}$$

where $\boldsymbol{u}$ is the solution vector, $\boldsymbol{f}$ is the hyperbolic part of the flux, and $\mathbf{D}$ is the diffusion tensor. Let $\partial\Omega \equiv \{0, 1\}$ be the boundary of the domain, $\Gamma_u \subset \partial\Omega$ is the part of the boundary where essential conditions are imposed, and $\Gamma_n \equiv \partial\Omega \backslash \Gamma_u$ is the part of the boundary with natural boundary conditions:

$$\boldsymbol{u} = \bar{\boldsymbol{u}} \quad \text{on } \Gamma_u, \tag{2}$$

$$(\boldsymbol{f} - \mathbf{D}\partial_x \boldsymbol{u})n = \overline{\boldsymbol{F}} \quad \text{on } \Gamma_n, \tag{3}$$

where n is the outward unit normal to the boundary, that is, $n = +1$ at $x = 1$, and $n = -1$ at $x = 0$. The initial conditions

$$\boldsymbol{u}(x, t = 0) = \boldsymbol{u}_0(x), \quad x \in \bar{\Omega} \equiv [0, 1], \tag{4}$$

close the definition of the mathematical problem.

2.2. Weak form

We define the following functional spaces:

$$\mathscr{V} := \{\boldsymbol{v} \in W : \boldsymbol{v} = \bar{\boldsymbol{u}} \text{ on } \Gamma_u\},$$
$$\mathscr{V}_0 := \{\boldsymbol{v} \in W : \boldsymbol{v} = \boldsymbol{0} \text{ on } \Gamma_u\},$$

where the appropriate Sobolev space W depends on the particular form of the diffusion tensor. The weak form of problem (1)–(4) consists in finding $\boldsymbol{u} \in \mathscr{V}$ for each fixed $t \in (0, T]$, such that

$$\begin{aligned} &(\partial_t \boldsymbol{u}, \boldsymbol{v}) + a(\boldsymbol{u}, \boldsymbol{v}; \boldsymbol{u}) = l(\boldsymbol{v}) \quad \forall \boldsymbol{v} \in \mathscr{V}_0, \\ &\boldsymbol{u}(x, t = 0) = \boldsymbol{u}_0(x), \end{aligned} \tag{5}$$

where

$$(\partial_t \boldsymbol{u}, \boldsymbol{v}) = \int_\Omega \partial_t \boldsymbol{u} \cdot \boldsymbol{v} \, \mathrm{d}\Omega, \tag{6}$$

$$a(\boldsymbol{u}, \boldsymbol{v}; \boldsymbol{w}) = -\int_\Omega \boldsymbol{f}(\boldsymbol{w}) \cdot \partial_x \boldsymbol{v} \, \mathrm{d}\Omega + \int_\Omega \mathbf{D}(\boldsymbol{w}) \partial_x \boldsymbol{u} \cdot \partial_x \boldsymbol{v} \, \mathrm{d}\Omega, \tag{7}$$

$$l(\boldsymbol{v}) = -\int_{\Gamma_n} \overline{\boldsymbol{F}} \cdot \boldsymbol{v} \, \mathrm{d}\Gamma. \tag{8}$$

2.3. Classical Galerkin method

Consider conforming finite-dimensional spaces $\mathscr{V}_h \subset \mathscr{V}$ and $\mathscr{V}_{h,0} \subset \mathscr{V}_0$ of piece-wise polynomials, defined on a finite element mesh. The standard Galerkin approximation of (5) is simply to find $\boldsymbol{u}_h \in \mathscr{V}_h$ for each fixed t such that

$$(\partial_t \boldsymbol{u}_h, \boldsymbol{v}_h) + a(\boldsymbol{u}_h, \boldsymbol{v}_h; \boldsymbol{u}_h) = l(\boldsymbol{v}_h) \quad \forall \boldsymbol{v}_h \in \mathscr{V}_{h,0}, \tag{9}$$

and $\boldsymbol{u}_h(x, t = 0)$ is the projection of the initial function $\boldsymbol{u}_0(x)$ onto space $\mathscr{V}_h$. The system of ordinary differential equations (9) is transformed into a system of (nonlinear) algebraic equations by further discretizing the time derivative [41].

2.4. Multiple-scale approach

It is well-known that the classical Galerkin method lacks stability when diffusive effects are small. The objective of the multiple-scale approach described here is to obtain a stabilized numerical formulation for this type of problems. The variational multiscale formulation was originally introduced in [21].

The key idea of the formulation is to perform a multiscale split

$$\boldsymbol{u} = \boldsymbol{u}_h + \tilde{\boldsymbol{u}}, \tag{10}$$

where $\boldsymbol{u}_h$ is the resolved—grid—scale and $\tilde{\boldsymbol{u}}$ is the unresolved—subgrid—scale. By using this decomposition, we acknowledge that certain components of the solution cannot be captured by the finite element mesh. This is definitely the case in advection-dominated problems, where the solution develops sharp fronts that would require an impractical grid resolution. Decomposition (10) is unique if one can express the original functional space $\mathscr{V}$ as the direct sum of two spaces:

$$\mathscr{V} = \mathscr{V}_h \oplus \widetilde{\mathscr{V}}, \tag{11}$$

where $\mathscr{V}_h$ is the space of *resolved scales* and $\widetilde{\mathscr{V}}$ is the space of *subgrid scales*. The space $\mathscr{V}$ is an infinite-dimensional space that completes $\mathscr{V}_h$ in $\mathscr{V}$. This space is generally unknown, and it is the role of the subgrid model to provide a successful approximation to it.

The multiscale decomposition was originally proposed for the linear advection–diffusion equation in [21,22], and then extended to other linear [9,10,18,19,29,36–38] and nonlinear [11,12,16,17,26–28] problems. A common approach to deal with nonlinear problems is to linearize the equations upfront, using either a Picard or a Newton strategy [11,12]. In this work, however, we resort to the multiscale decomposition prior to any linearization. In the context of nonlinear problems, it seems natural to express the solution at a given iteration step (k) as

$$\boldsymbol{u}^{(k)} = \boldsymbol{u}^{(k-1)} + \delta\boldsymbol{u}^{(k-1)}. \tag{12}$$

The first term on the right-hand side should be understood as an approximate solution at the previous iteration level, and the second term as a correction. In principle, both terms are subject to the multiscale decomposition (10):

$$\boldsymbol{u}^{(k-1)} = \boldsymbol{u}_h^{(k-1)} + \tilde{\boldsymbol{u}}^{(k-1)}, \tag{13}$$

$$\delta\boldsymbol{u}^{(k-1)} = \delta\boldsymbol{u}_h^{(k-1)} + \delta\tilde{\boldsymbol{u}}^{(k-1)}, \tag{14}$$

Eq. (13) requires that the approximate solution $\boldsymbol{u}^{(k-1)}$ is reconstructed after every iteration. To avoid this reconstruction step, and obtain a formulation that completely decouples the resolved and unresolved scales (see below), we make the additional approximation:

$$\boldsymbol{u}^{(k-1)} \approx \boldsymbol{u}_h^{(k-1)}, \tag{15}$$

so that the multiscale split takes the form:

$$\boldsymbol{u}^{(k)} \approx \boldsymbol{u}_h^{(k)} + \delta\tilde{\boldsymbol{u}}^{(k-1)}. \tag{16}$$

In what follows we shall drop superscripts referring to the iteration level, and simply write

$$\boldsymbol{u} \approx \boldsymbol{u}_h + \delta\tilde{\boldsymbol{u}} \tag{17}$$

Remarks.

1. We refer to Eq. (17) as an incremental formulation, with a multiscale decomposition of the increment.
2. The term $\boldsymbol{u}_h$ in Eq. (17) should be understood as an approximate solution about which the equations are linearized. The term $\delta\tilde{\boldsymbol{u}}$ plays the role of a perturbation that will allow stabilization of the solution.
3. The working assumption (15) makes our formulation different from that in [12] and [16,17], where the subgrid scales are tracked, and the multiscale variable is reconstructed after every step of the iterative process.

The derivation of the multiscale formulation starts by invoking a multi-scale split of the solution $\boldsymbol{u}$ and the test function $\boldsymbol{v}$:

$$\boldsymbol{u} = \boldsymbol{u}_h + \delta\tilde{\boldsymbol{u}} \in \mathscr{V} = \mathscr{V}_h \oplus \widetilde{\mathscr{V}}, \tag{18}$$

$$\boldsymbol{v} = \boldsymbol{v}_h + \tilde{\boldsymbol{v}} \in \mathscr{V}_0 = \mathscr{V}_{h,0} \oplus \widetilde{\mathscr{V}}. \tag{19}$$

Because the weak form is linear with respect to the test function $\boldsymbol{v}$, the original mathematical problem (5) is split into two, a grid scale problem:

$$(\partial_t(\boldsymbol{u}_h + \delta\tilde{\boldsymbol{u}}), \boldsymbol{v}_h) + a(\boldsymbol{u}_h + \delta\tilde{\boldsymbol{u}}, \boldsymbol{v}_h; \boldsymbol{u}_h + \delta\tilde{\boldsymbol{u}}) = l(\boldsymbol{v}_h) \quad \forall \boldsymbol{v}_h \in \mathscr{V}_{h,0}, \tag{20}$$

and a subscale problem:

$$(\partial_t(\boldsymbol{u}_h + \delta\tilde{\boldsymbol{u}}), \tilde{\boldsymbol{v}}) + a(\boldsymbol{u}_h + \delta\tilde{\boldsymbol{u}}, \tilde{\boldsymbol{v}}; \boldsymbol{u}_h + \delta\tilde{\boldsymbol{u}}) = l(\tilde{\boldsymbol{v}}) \quad \forall \tilde{\boldsymbol{v}} \in \widetilde{\mathscr{V}}. \tag{21}$$

2.4.1. Subgrid scale problem

We write the flux term in (21) as a sum of element integrals, and we integrate by parts on each element:

$$\begin{aligned} a(\boldsymbol{u}_h + \delta\tilde{\boldsymbol{u}}, \tilde{\boldsymbol{v}}; \boldsymbol{u}_h + \delta\tilde{\boldsymbol{u}}) &= -\sum_e \int_{\Omega^e} (\boldsymbol{f}(\boldsymbol{u}_h + \delta\tilde{\boldsymbol{u}}) - \mathbf{D}(\boldsymbol{u}_h + \delta\tilde{\boldsymbol{u}})\partial_x(\boldsymbol{u}_h + \delta\tilde{\boldsymbol{u}})) \cdot \partial_x\tilde{\boldsymbol{v}}\,\mathrm{d}\Omega \\ &= \sum_e \int_{\Omega^e} \partial_x(\boldsymbol{f}(\boldsymbol{u}_h + \delta\tilde{\boldsymbol{u}}) - \mathbf{D}(\boldsymbol{u}_h + \delta\tilde{\boldsymbol{u}})\partial_x(\boldsymbol{u}_h + \delta\tilde{\boldsymbol{u}})) \cdot \tilde{\boldsymbol{v}}\,\mathrm{d}\Omega \\ &\quad - \sum_e \int_{\Gamma^e} (\boldsymbol{f}(\boldsymbol{u}_h + \delta\tilde{\boldsymbol{u}}) - \mathbf{D}(\boldsymbol{u}_h + \delta\tilde{\boldsymbol{u}})\partial_x(\boldsymbol{u}_h + \delta\tilde{\boldsymbol{u}}))n \cdot \tilde{\boldsymbol{v}}\,\mathrm{d}\Gamma. \end{aligned} \tag{22}$$

We assume continuity of the flux across interelement boundaries, so that the boundary integrals cancel each other on adjacent elements in the interior of the domain, that is,

$$-\sum_e \int_{\Gamma^e} (\boldsymbol{f}(\boldsymbol{u}_h + \delta\tilde{\boldsymbol{u}}) - \mathbf{D}(\boldsymbol{u}_h + \delta\tilde{\boldsymbol{u}})\partial_x(\boldsymbol{u}_h + \delta\tilde{\boldsymbol{u}}))n \cdot \tilde{\boldsymbol{v}}\,\mathrm{d}\Gamma \approx -\int_{\Gamma_n} \overline{\boldsymbol{F}} \cdot \tilde{\boldsymbol{v}}\,\mathrm{d}\Gamma \equiv l(\bar{\boldsymbol{v}}). \tag{23}$$

The expression above is a true identity if $\boldsymbol{u}_h + \delta\tilde{\boldsymbol{u}}$ is the exact solution, or if locally mass conservative finite element spaces are employed. Otherwise, Eq. (23) should be regarded as an approximation.

We now approximate the total flux by a first-order Taylor expansion about the coarse-scale solution $\boldsymbol{u}_h$:

$$\begin{aligned} \boldsymbol{f}(\boldsymbol{u}_h + \delta\tilde{\boldsymbol{u}}) - \mathbf{D}(\boldsymbol{u}_h + \delta\tilde{\boldsymbol{u}})\partial_x(\boldsymbol{u}_h + \delta\tilde{\boldsymbol{u}}) &= \boldsymbol{f}(\boldsymbol{u}_h) - \mathbf{D}(\boldsymbol{u}_h)\partial_x\boldsymbol{u}_h \\ &\quad + \boldsymbol{f}'(\boldsymbol{u}_h)\delta\tilde{\boldsymbol{u}} - (\mathbf{D}'(\boldsymbol{u}_h)\delta\tilde{\boldsymbol{u}})\partial_x\boldsymbol{u}_h - \mathbf{D}(\boldsymbol{u}_h)\partial_x(\delta\tilde{\boldsymbol{u}}) + \mathrm{O}(|\delta\tilde{\boldsymbol{u}}|^2). \end{aligned} \tag{24}$$

Eq. (24) suggests defining the *linearized* advection–diffusion operator in conservation form:

$$\mathscr{L}_{u_h}\boldsymbol{v} := \partial_x[\boldsymbol{f}'(\boldsymbol{u}_h)\boldsymbol{v} - (\mathbf{D}'(\boldsymbol{u}_h)\boldsymbol{v})\partial_x\boldsymbol{u}_h - \mathbf{D}(\boldsymbol{u}_h)\partial_x\boldsymbol{v}]. \tag{25}$$

The operator $\mathscr{L}_{u_h}\boldsymbol{v}$ depends in a nonlinear fashion on the approximate coarse-scale solution $\boldsymbol{u}_h$, but is linear in its argument $\boldsymbol{v}$. We write this operator in the more suggestive (and convenient) form:

$$\mathscr{L}_{u_h}\boldsymbol{v} := \partial_x[\mathbf{A}(\boldsymbol{u}_h)\boldsymbol{v} - \mathbf{D}(\boldsymbol{u}_h)\partial_x\boldsymbol{v}]. \tag{26}$$

where $\mathbf{A}(\boldsymbol{u}_h)$ is an "advection" operator, whose components $A_{ij}(\boldsymbol{u}_h)$ take the following expression:

$$A_{ij}(\boldsymbol{u}_h) := \frac{\partial f_i(\boldsymbol{u}_h)}{\partial u_{h,j}} - \sum_k \frac{\partial D_{ik}(\boldsymbol{u}_h)}{\partial u_{h,j}}\partial_x u_{h,k}. \tag{27}$$

Using Eqs. (23)–(26) in Eq. (22), we write the first-order approximation of the flux term in the subgrid scale problem (21) as

$$\begin{aligned} a(\boldsymbol{u}_h + \delta\tilde{\boldsymbol{u}}, \tilde{\boldsymbol{v}}; \boldsymbol{u}_h + \delta\tilde{\boldsymbol{u}}) \approx & \sum_e \int_{\Omega^e} \partial_x(\boldsymbol{f}(\boldsymbol{u}_h) - \mathbf{D}(\boldsymbol{u}_h)\partial_x\boldsymbol{u}_h)\cdot\tilde{\boldsymbol{v}}\,\mathrm{d}\Omega \\ & + \sum_e \int_{\Omega^e} \mathscr{L}_{u_h}\delta\tilde{\boldsymbol{u}}\cdot\tilde{\boldsymbol{v}}\,\mathrm{d}\Omega - \int_{\Gamma_n}\bar{\mathbf{F}}\cdot\tilde{\boldsymbol{v}}\,\mathrm{d}\Gamma. \end{aligned} \tag{28}$$

A further approximation is to consider *quasi-static subscales* [12]:

$$\partial_t\delta\tilde{\boldsymbol{u}} \approx 0. \tag{29}$$

After this final assumption, and defining the *grid-scale residual*

$$\mathscr{R}(\boldsymbol{u}_h) := -\partial_t\boldsymbol{u}_h - \partial_x(\boldsymbol{f}(\boldsymbol{u}_h) - \mathbf{D}(\boldsymbol{u}_h)\partial_x\boldsymbol{u}_h), \tag{30}$$

the subscale problem (21) is written as follows:

$$\sum_e \int_{\Omega^e} \mathscr{L}_{u_h}\delta\tilde{\boldsymbol{u}}\cdot\tilde{\boldsymbol{v}}\,\mathrm{d}\Omega = \sum_e \int_{\Omega^e} \mathscr{R}(\boldsymbol{u}_h)\cdot\tilde{\boldsymbol{v}}\,\mathrm{d}\Omega \quad \forall\tilde{\boldsymbol{v}} \in \widetilde{\mathscr{V}}. \tag{31}$$

Eq. (31) illustrates that the subgrid scale problem is in fact a projection problem:

$$\widetilde{\Pi}(\mathscr{L}_{u_h}\delta\tilde{\boldsymbol{u}}) = \widetilde{\Pi}(\mathscr{R}(\boldsymbol{u}_h)), \tag{32}$$

where $\widetilde{\Pi}$ is the L^2-projection onto the space of subgrid scales $\widetilde{\mathscr{V}}$.

Remarks.

1. The subgrid scale problem is infinite-dimensional, so one cannot expect to solve it exactly. It is necessary to resort to some kind of numerical or analytical approximation.
2. To reduce dramatically the computational cost of the solution to the subscale problem, it seems appealing to *localize* the problem, so that it can be approximated element by element. The difficulty of this step stems from the fact that the boundary conditions of the local problem—values of the subscales on the inter-element boundaries—are unknown. A common modeling assumption is to use bubble functions, that is, subscales that vanish on the boundaries of each element [4,5,14,21].
3. An alternative to assumption (29) of quasi-static subscales is to track the value of the subscales in every element [12].

In this paper we employ an algebraic approximation to the subscales, which leads to an algebraic subgrid scale model (ASGS):

$$\delta\tilde{\boldsymbol{u}} \approx \boldsymbol{\tau}_{u_h}\mathscr{R}(\boldsymbol{u}_h), \tag{33}$$

where $\boldsymbol{\tau}_{u_h}$ is a matrix of algebraic coefficients, which depend not only on the system parameters, but also on the grid scale solution $\boldsymbol{u}_h$. This approximation is substantiated by the convergence analysis of the linear case [13]. It can also be justified from an asymptotic Fourier analysis [13], and has proven useful in numerical tests. The matrix $\boldsymbol{\tau}_{u_h}$ is known as the matrix of stabilizing coefficients or matrix of intrinsic time scales [23], and has dimension of time. Its design, which should be dictated ultimately by stability and convergence analysis, is one of the most difficult issues in the development of a stabilized numerical method. Many alternatives have been proposed, some of which are reviewed and succinctly described in Section 2.5.

2.4.2. Grid scale problem

We linearize the flux term in Eq. (20) with respect to the coarse scale solution $\boldsymbol{u}_h$:

$$\begin{aligned} a(\boldsymbol{u}_h+\delta\tilde{\boldsymbol{u}},\boldsymbol{v}_h;\boldsymbol{u}_h+\delta\tilde{\boldsymbol{u}}) &= -\int_\Omega (\boldsymbol{f}(\boldsymbol{u}_h+\delta\tilde{\boldsymbol{u}})-\mathbf{D}(\boldsymbol{u}_h+\delta\tilde{\boldsymbol{u}})\partial_x(\boldsymbol{u}_h+\delta\tilde{\boldsymbol{u}}))\cdot\partial_x\boldsymbol{v}_h\,\mathrm{d}\Omega \\ &= -\int_\Omega (\boldsymbol{f}(\boldsymbol{u}_h)-\mathbf{D}(\boldsymbol{u}_h)\partial_x\boldsymbol{u}_h)\cdot\partial_x\boldsymbol{v}_h\,\mathrm{d}\Omega \\ &\quad -\int_\Omega (\boldsymbol{f}'(\boldsymbol{u}_h)\delta\tilde{\boldsymbol{u}}-(\mathbf{D}'(\boldsymbol{u}_h)\delta\tilde{\boldsymbol{u}})\partial_x\boldsymbol{u}_h)\cdot\partial_x\boldsymbol{v}_h\,\mathrm{d}\Omega \\ &\quad +\int_\Omega (\mathbf{D}(\boldsymbol{u}_h)\partial_x\delta\tilde{\boldsymbol{u}})\cdot\partial_x\boldsymbol{v}_h\,\mathrm{d}\Omega+\mathrm{O}(|\delta\tilde{\boldsymbol{u}}|^2). \end{aligned} \tag{34}$$

The first term in the final expression of (34) is the Galerkin term:

$$-\int_\Omega (\boldsymbol{f}(\boldsymbol{u}_h)-\mathbf{D}(\boldsymbol{u}_h)\partial_x\boldsymbol{u}_h)\cdot\partial_x\boldsymbol{v}_h\,\mathrm{d}\Omega = a(\boldsymbol{u}_h,\boldsymbol{v}_h;\boldsymbol{u}_h). \tag{35}$$

Writing the second integral in (34) as a sum of element integrals, and recalling the expression of the linearized "advection" matrix (27), we get

$$-\int_\Omega (\boldsymbol{f}'(\boldsymbol{u}_h)\delta\tilde{\boldsymbol{u}}-(\mathbf{D}'(\boldsymbol{u}_h)\delta\tilde{\boldsymbol{u}})\partial_x\boldsymbol{u}_h)\cdot\partial_x\boldsymbol{u}_h\,\mathrm{d}\Omega = \sum_e \int_{\Omega^e} (-\mathbf{A}^{\mathrm{T}}(\boldsymbol{u}_h)\partial_x\boldsymbol{v}_h)\cdot\delta\tilde{\boldsymbol{u}}\,\mathrm{d}\Omega, \tag{36}$$

where $\mathbf{A}^{\mathrm{T}}$ is the transpose of $\mathbf{A}$. After integration by parts element by element, the third term in (34) is written as

$$\int_\Omega (\mathbf{D}(\boldsymbol{u}_h)\partial_x\delta\tilde{\boldsymbol{u}})\cdot\partial_x\boldsymbol{v}_h\,\mathrm{d}\Omega = -\sum_e \int_{\Omega^e} \partial_x(\mathbf{D}^{\mathrm{T}}(\boldsymbol{u}_h)\partial_x\boldsymbol{v}_h)\cdot\delta\tilde{\boldsymbol{u}}\,\mathrm{d}\Omega+\sum_e\int_{\Gamma^e}(\mathbf{D}^{\mathrm{T}}(\boldsymbol{u}_h)\partial_x\boldsymbol{v}_h)n\cdot\delta\tilde{\boldsymbol{u}}\,\mathrm{d}\Gamma. \tag{37}$$

Defining the *adjoint* of the linearized advection–diffusion operator (26),

$$\mathscr{L}^*_{u_h}\boldsymbol{v} := -\mathbf{A}^{\mathrm{T}}(\boldsymbol{u}_h)\partial_x\boldsymbol{v}-\partial_x(\mathbf{D}^{\mathrm{T}}(\boldsymbol{u}_h)\partial_x\boldsymbol{v}), \tag{38}$$

and its associated *boundary operator*,

$$\mathbf{b}^*_{u_h}\boldsymbol{v} := (\mathbf{D}^{\mathrm{T}}(\boldsymbol{u}_h)\partial_x\boldsymbol{v})n, \tag{39}$$

and substituting (35)–(37) in Eq. (34), the flux term of the grid scale equation takes the form:

$$a(\boldsymbol{u}_h+\delta\tilde{\boldsymbol{u}},\boldsymbol{v}_h;\boldsymbol{u}_h+\delta\tilde{\boldsymbol{u}}) = a(\boldsymbol{u}_h,\boldsymbol{v}_h,\boldsymbol{u}_h)+\sum_e\int_{\Omega^e}\mathscr{L}^*_{u_h}\boldsymbol{v}_h\cdot\delta\tilde{\boldsymbol{u}}\,\mathrm{d}\Omega+\sum_e\int_{\Gamma^e}\boldsymbol{b}^*_{u_h}\boldsymbol{v}_h\cdot\delta\tilde{\boldsymbol{u}}\,\mathrm{d}\Gamma+\mathrm{O}(|\delta\tilde{\boldsymbol{u}}|^2). \tag{40}$$

Substituting the first-order approximation of (40) in (20), and considering quasi-static subscales as before, we obtain the final form of the grid scale equation:

$$(\partial_t\boldsymbol{u}_h,\boldsymbol{v}_h)+a(\boldsymbol{u}_h,\boldsymbol{v}_h;\boldsymbol{u}_h)+\sum_e\int_{\Omega^e}\mathscr{L}^*_{u_h}\boldsymbol{v}_h\cdot\delta\tilde{\boldsymbol{u}}\,\mathrm{d}\Omega+\sum_e\int_{\Gamma^e}\boldsymbol{b}^*_{u_h}\boldsymbol{v}_h\cdot\delta\tilde{\boldsymbol{u}}\,\mathrm{d}\Gamma = l(\boldsymbol{v}_h)\quad\forall\boldsymbol{v}_h\in\mathscr{V}_{h,0}. \tag{41}$$

Remarks.

1. By direct comparison with (9), it is immediate to identify in Eq. (41) the Galerkin terms and the additional stabilizing terms of the multiscale formulation.
2. The stabilizing terms are evaluated element by element, and consist of a volume integral and a boundary integral. The boundary contribution to the stabilizing term is neglected in the numerical simulations of Sections 3 and 4. This simplification is sensible only if the magnitude of the diffusive effects is small, which is precisely the case of interest.
3. The grid scale Eq. (41) and the subgrid scale Eq. (31) are coupled through the value of the subscales $\delta\tilde{\boldsymbol{u}}$. For the simple sub-grid scale model employed here, the algebraic approximation (33) is substituted in Eq. (41).
4. Because the subscales are proportional to the grid-scale residual—Eq. (33), the formulation is residual-based and, therefore, automatically consistent.
5. The key features of the formulation are the following:
   (a) Linearization of the equations is employed *after* the multiscale split. In particular, only the subscale effects are linearized, whereas the full nonlinear Galerkin term is retained in the grid scale equation.
   (b) The approximate solution is *not* reconstructed after every step in the iterative process, or even after every time step. The benefit of this working assumption is that subscale effects enter the formulation in an integral sense only.

2.5. Matrix of stabilizing coefficients

The description of the multiscale finite element formulation is complete up to the definition of the matrix of stabilizing coefficients $\boldsymbol{\tau}_{u_h}$. Here we review briefly several options that have been considered in the literature. They all define the stabilization matrix $\boldsymbol{\tau}$ for the *linear* advection–diffusion problem. Extension to the nonlinear problem is straightforward, after defining the *linearized* advection–diffusion operator (26).

2.5.1. Definition through an eigenvalue problem

This formulation was originally developed in [23]. The idea is to start from the formulation of the scalar one-dimensional linear advection–diffusion equation [6]—for which it is possible to define a function τ so that the numerical solution is nodally exact—and extend it to systems of equations in multidimensions. The basis for such extension is to diagonalize the system of equations, by solving an eigenvalue problem, and transform the matrix of stabilizing coefficients accordingly.

For one-dimensional problems, the matrix of stabilizing coefficients is given by [10,23]:

$$\boldsymbol{\tau}_{u_h} = \mathbf{R}\hat{\boldsymbol{\tau}}_{u_h}\mathbf{R}^{\mathrm{T}}, \tag{42}$$

where $\mathbf{R} = [\boldsymbol{r}_1, \ldots, \boldsymbol{r}_n]$. We denote by v_i, $\boldsymbol{r}_i$, the eigenvalues and eigenvectors of the advection matrix $\mathbf{A}$, respectively, and

$$\hat{\boldsymbol{\tau}}_{u_h} = \mathrm{diag}(\hat{\tau}_1, \ldots, \hat{\tau}_n). \tag{43}$$

Each intrinsic time is defined as

$$\hat{\tau}_i = \frac{1}{2} h \frac{\hat{\xi}(\alpha_i)}{|v_i|}, \tag{44}$$

where h is the size of the element, α_i is a measure of the element Peclet number for the ith equation,

$$\alpha_i = \frac{1}{2}\frac{|v_i|h}{\epsilon_i}, \quad \epsilon_i = \boldsymbol{r}_i^{\mathrm{T}}\mathbf{D}\boldsymbol{r}_i. \tag{45}$$

and $\hat{\xi}$ is a diffusion correction factor given by

$$\hat{\xi}(\alpha) = \coth(\alpha) - \frac{1}{\alpha}. \tag{46}$$

Alternative definitions of the diffusion corrector factor $\hat{\xi}$ have been proposed [40].

The formulation of the matrix $\boldsymbol{\tau}$ described here applies also to the nonlinear advection–diffusion operator (26). In this case, the advection and diffusion matrices are not constant, but functions of the solution itself. Therefore, an eigenvalue problem needs to be solved at each integration point.

2.5.2. Definition through the matrix inverse

A different design of the matrix of intrinsic time scales was proposed in [10] for systems of advection–diffusion–reaction equations in multidimensions. When restricted to one-dimensional systems of advection–diffusion type, the expression of $\boldsymbol{\tau}_{u_h}$ reduces to

$$\boldsymbol{\tau}_{u_h} = \left(\frac{c_1}{h^2} \mathbf{D}(\boldsymbol{u}_h) + \frac{c_2}{h} \mathbf{A}(\boldsymbol{u}_h) \right)^{-1}, \tag{47}$$

where $c_1 = 4$ and $c_2 = 2$ for linear elements. This expression emanates from an analysis of the discrete maximum principle in the scalar, stationary, one-dimensional case [9,10]. The matrix $\boldsymbol{\tau}$ given by (47) is a matrix function of the advection and diffusion matrices, which is the essential requirement for the method to provide optimal stabilization for each individual scalar equation when the system is diagonalized [10].

2.6. Shock-capturing techniques

While the multiscale formulation described above will produce stabilized numerical solutions, overshoots and undershoots may still remain in the neighborhood of internal and boundary layers. The reason for this localized oscillatory behavior is that the method does not guarantee monotonic solutions. One possibility to enhance the robustness of the stabilized formulation is to incorporate a discontinuity-capturing term, that will further reduce or completely eliminate spurious numerical oscillations.

Many of the existing discontinuity-capturing formulations can be expressed as an extra diffusion term [8],

$$\sum_e \int_{\Omega^e} \mathbf{D}_{\mathrm{sc}}(\boldsymbol{u}_h) \partial_x \boldsymbol{u}_h \cdot \partial_x \boldsymbol{v}_h \, \mathrm{d}\Omega, \tag{48}$$

where the numerical diffusion tensor $\mathbf{D}_{\mathrm{sc}}$ depends on the coarse scale solution. This term leads necessarily to a nonlinear method, even if the underlying equation is linear.

The "canonical" form of the discontinuity-capturing diffusion is

$$D_{\mathrm{sc,1}} = \frac{1}{2} h \frac{|\mathscr{R}(\boldsymbol{u}_h)|}{|\partial_x \boldsymbol{u}_h|}. \tag{49}$$

We propose a different expression, where the local gradient $\partial_x \boldsymbol{u}_h$ is replaced by a global measure of the gradient $\sim \boldsymbol{U}_{\mathrm{sc}}/h$:

$$D_{\mathrm{sc,g}} = C_{\mathrm{sc}} h \frac{|\mathscr{R}(\boldsymbol{u}_h)|}{|\boldsymbol{U}_{\mathrm{sc}}/h|}, \tag{50}$$

where C_{sc} is a constant coefficient and U_{sc} is a constant vector of characteristic values of the solution. The main effect of expression (50) is to introduce less diffusion where the gradient of the solution is small.

3. Three-phase flow in porous media

In this section we apply the variational multiscale formulation to the one-dimensional three-phase flow in porous media. We review briefly the standard mathematical model, and we present numerical simulations that show the performance of the multiscale method.

3.1. Mathematical formulation

Under fairly standard assumptions, the mathematical problem can be expressed as a pressure equation of elliptic type, and a system of saturation equations of parabolic type [3,7,30]. The solution to the pressure equation is trivial in the one-dimensional case, and we concentrate exclusively on the system of saturation equations which, in dimensionless variables, takes the form of system (1):

$$\partial_t \boldsymbol{u} + \partial_x \boldsymbol{f} - \partial_x(\mathbf{D}\partial_x \boldsymbol{u}) = \mathbf{0}, \tag{51}$$

where

$$\boldsymbol{u} := \begin{pmatrix} S_w \\ S_g \end{pmatrix}, \tag{52}$$

$$\boldsymbol{f} := \begin{pmatrix} f_w \\ f_g \end{pmatrix}, \tag{53}$$

$$\mathbf{D} := \begin{pmatrix} D_{ww} & D_{wg} \\ D_{gw} & D_{gg} \end{pmatrix} = \begin{pmatrix} \epsilon_w \lambda_w (1-f_w) \dfrac{\mathrm{d}P^D_{cw}}{\mathrm{d}S_w} & -\epsilon_g \lambda_w f_g \dfrac{\mathrm{d}P^D_{cg}}{\mathrm{d}S_g} \\ -\epsilon_w \lambda_g f_w \dfrac{\mathrm{d}P^D_{cw}}{\mathrm{d}S_w} & \epsilon_g \lambda_g (1-f_g) \dfrac{\mathrm{d}P^D_{cg}}{\mathrm{d}S_g} \end{pmatrix} \tag{54}$$

are the vector of water and gas normalized saturations, the fractional flow vector and the capillary-diffusion tensor, respectively. The fractional flow of the α-phase is

$$f_\alpha := \frac{\lambda_\alpha}{\lambda_\mathrm{T}}, \quad \lambda_\mathrm{T} = \sum_{\alpha=w,o,g} \lambda_\alpha, \tag{55}$$

where λ_α is the mobility of the α-phase, and λ_T is the total mobility (sum of water, oil, and gas mobilities). The phase mobility is

$$\lambda_\alpha := \frac{k_{r\alpha}}{\mu_\alpha}, \tag{56}$$

where $k_{r\alpha}$ is the relative permeability and μ_α is the dynamic viscosity of the α-phase. The function $P^D_{c\alpha}$ denotes a dimensionless capillary pressure of the α-phase, and ϵ_α a capillary number (see [30] for details).

Therefore, the fractional flow vector and the diffusion tensor are nonlinear functions of the fluid saturations:

$$\boldsymbol{f} = \boldsymbol{f}(\boldsymbol{u}), \quad \mathbf{D} = \mathbf{D}(\boldsymbol{u}). \tag{57}$$

The character of the system (51) depends on the eigenvalues and eigenvectors of the Jacobian matrix $\boldsymbol{f}'$. In previous work [34], we derived conditions on the relative permeability functions that guarantee that the eigenvalues of the Jacobian matrix are everywhere real and distinct. Here, we further assume that the capillary diffusion tensor is positive semi-definite. Under these conditions, the system of equations is parabolic, and strictly hyperbolic in the limit of vanishing diffusion.

3.2. Numerical simulations

We present several simulations of one-dimensional three-phase flow. For the sole purpose of testing the formulation, the capillary diffusion tensor is taken as a constant diagonal matrix, that is, Eq. (54) is replaced by

$$\mathbf{D} = \begin{pmatrix} \epsilon_w & 0 \\ 0 & \epsilon_g \end{pmatrix}. \tag{58}$$

The *form* of the capillary diffusion tensor may affect the detailed structure of individual shocks, but not the shock location and the global structure of the solution. We are interested in the nearly hyperbolic case, so we shall use very small values of the capillary diffusion coefficients ϵ_w, ϵ_g.

We use the following relative permeability functions [32]:

$$\begin{aligned} k_{rw} &= S_w^2, \\ k_{ro} &= (1 - S_w)(1 - S_g)(1 - S_w - S_g), \\ k_{rg} &= \beta_g S_g + (1 - \beta_g) S_g^2, \end{aligned} \tag{59}$$

with $\beta_g = 0.1$, and the following values of the fluid viscosities:

$$\mu_w = 0.875, \quad \mu_g = 0.03, \quad \mu_o = 2. \tag{60}$$

We reproduce approximately the conditions of the Riemann problem by imposing the constant initial condition $\boldsymbol{u}(x, 0) = \boldsymbol{u}_r$, and a Dirichlet boundary condition $\boldsymbol{u}(0, t) = \boldsymbol{u}_l$ on the left boundary. An analytical solution exists for the capillarity-free case, which can be used to verify the numerical solutions [32].

We study two scenarios: the first one involving oil filtration in a relatively dry soil, and the second one reproducing water–gas injection in an oil reservoir.

3.2.1. Oil filtration in relatively dry soil

This example reproduces filtration of a mixture of oil, water and gas through a relatively dry porous medium with some water and oil. The medium has the following initial normalized saturations: $S_w = 0.15$, $S_g = 0.8$, and $S_o = 0.05$. Fluids are injected in a proportion such that the normalized fluid saturations at the inlet face are: $S_w = 0.25$, $S_g = 0.2$, and $S_o = 0.55$. From a practical viewpoint, this problem could represent a contamination event in the shallow subsurface, under one-dimensional flow conditions.

Analytical solution. The exact solution to the capillarity-free problem consists in a sequence of two genuine shocks [32]. In Fig. 1 we show the profiles of water, gas, and oil saturations against the similarity variable $\zeta = x/t$. The solution at different times can be obtained from one another by simple stretching. The saturations at the right boundary coincide with the initial state, and the saturations at the left boundary correspond to the injected state. This figure illustrates the behavior of the displacement process: essentially, the oil phase displaces the water phase, which in turn displaces gas out of the porous medium.

"*Reference*" *numerical solution*. We test whether the numerical solution to the three-phase oil filtration problem *with capillarity* provides an accurate approximation to the analytical solution of the capillarity-free case above. We take small values of the capillary diffusion coefficients in Eq. (58):

$$\epsilon_w = 0.0005, \quad \epsilon_g = 0.001. \tag{61}$$

We compute a "reference" numerical solution using the standard Galerkin method on a very fine mesh of 4000 elements. We use a Crank–Nicolson time integration technique with a constant time step of $\delta t = 10^{-4}$. Given this discretization and the physical parameters of the problem—in particular the speed of propagation $\sigma_{\max}$ of the fast shock, we may define the following dimensionless parameters:

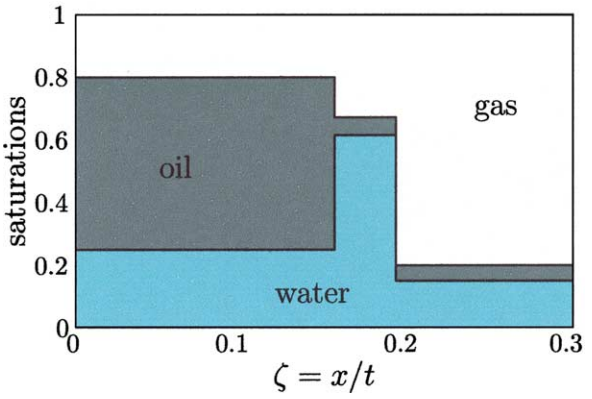

Fig. 1. Saturation profiles of the *exact solution* to the oil filtration problem. Saturations of each phase are plotted against the similarity variable $\zeta = x/t$.

$$Pe := \frac{\sigma_{\max} h}{\epsilon_{\min}} \approx 0.1 \quad \text{(element Peclet number)}, \tag{62}$$

$$Co := \frac{\sigma_{\max} \delta t}{h} \approx 0.08 \quad \text{(element Courant number)}. \tag{63}$$

The space and time discretization have been chosen to obtain small values of these two key parameters ($Pe \ll 1$, $Co \ll 1$), so that the reference solution given by the classical Galerkin method is stable and accurate. The comparison between this solution and the analytical solution described above is presented in Fig. 2 at time $t = 3$. The "reference" numerical solution captures correctly the global structure of the capillarity-free solution: the location of shocks and the magnitude of the intermediate constant state are predicted accurately. Further numerical simulations—using different values of the capillary diffusion coefficients and different number of elements—confirm that the standard Galerkin solution converges to the entropy solution of the capillarity-free problem.

Standard Galerkin solution. The same problem is solved using the standard Galerkin method on a coarse mesh of only 40 elements. The element Peclet number is now $Pe \approx 10$. A Crank–Nicolson time-stepping with $\delta t = 0.01$ is used. The associated Courant number is still very small ($Co \approx 0.08$), to minimize the

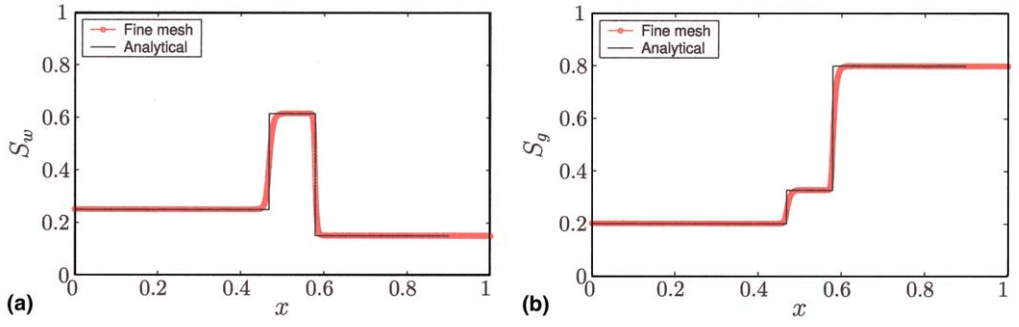

Fig. 2. Saturation profiles of the standard Galerkin solution to the oil filtration problem on a fine mesh of 4000 elements, and comparison to the analytical solution of the capillarity-free case. Results are shown at time $t = 3$. (a) Water saturation and (b) gas saturation.

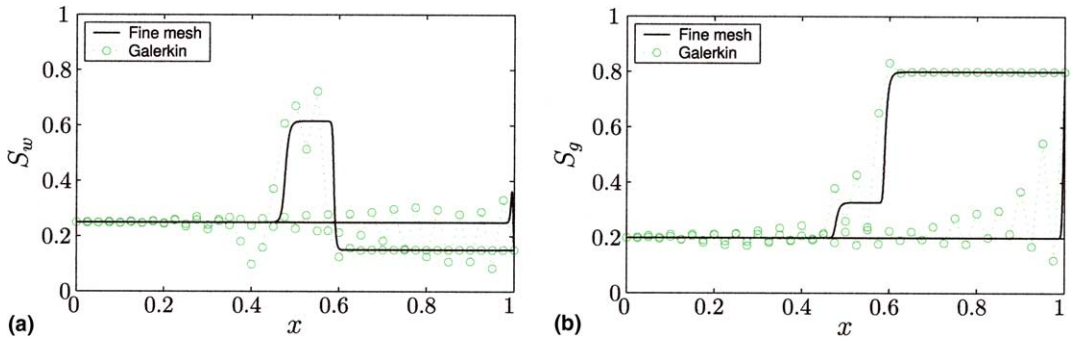

Fig. 3. Saturation profiles of the standard Galerkin solution to the oil filtration problem on a coarse mesh of 40 elements. Results are shown at times $t = 3$ and $t = 8$. (a) Water saturation and (b) gas saturation.

numerical error introduced by the time discretization. The results of this simulation are shown in Fig. 3. The solution obtained with the classical Galerkin method on a fine mesh of 4000 elements is included for reference. Water and gas saturation profiles are plotted at two different times: $t = 3$ (transient conditions), and $t = 8$ (quasi-steady conditions). It is apparent that the standard Galerkin solution on a coarse grid lacks stability, and is polluted with spurious oscillations. The instabilities are especially severe for the long-term solution, where the oscillatory behavior spreads over most of the computational domain.

Algebraic subgrid scale solutions. In Fig. 4 we plot the results obtained with the ASGS method and the definition of $\boldsymbol{\tau}$ given by the eigenvalue problem (42) (formulation proposed by Hughes and Mallet [23]). The solution is much stabler than the standard Galerkin solution. The computed saturation profiles do not display global oscillatory behavior, and capture sharply the transient shocks and the stationary boundary layers. Some small overshoots and undershoots remain, however, but they are confined to the vicinity of the sharp features in the solution.

The ASGS solution obtained with the $\boldsymbol{\tau}$ matrix given by the matrix inverse (47) (formulation proposed by Codina [10]) is shown in Fig. 5. The solution is virtually identical to that of Fig. 4, and the same comments apply.

Stabilized solutions with shock capturing diffusion. In an attempt to remove the localized wiggles that remain in the solution of the stabilized ASGS method, we test several shock-capturing techniques. We compare different expressions of the discontinuity-capturing diffusion applied to the same ASGS method. In this case, we choose the solution obtained with the $\boldsymbol{\tau}$ matrix of Hughes and Mallet [23] (Fig. 4).

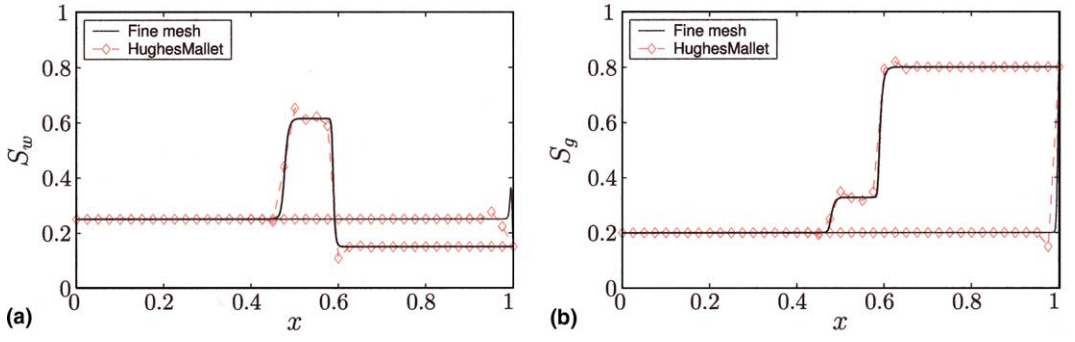

Fig. 4. Saturation profiles of the ASGS solution ($\boldsymbol{\tau}$ formulation given by Hughes and Mallet [23]) to the oil filtration problem on the coarse mesh. (a) Water saturation and (b) gas saturation.

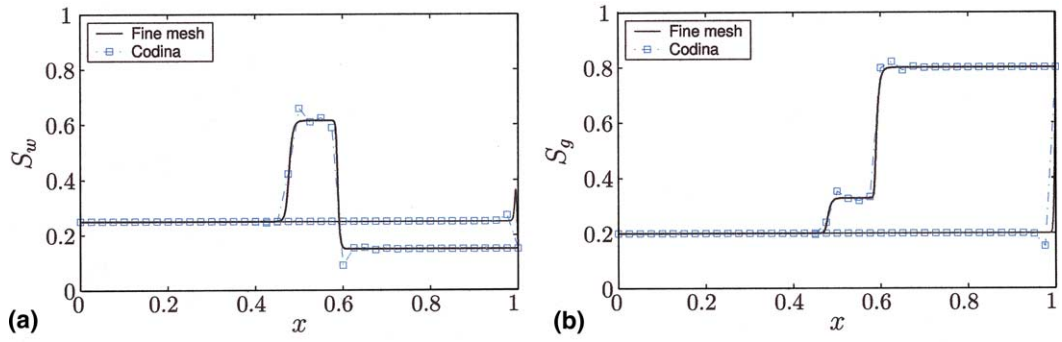

Fig. 5. Saturation profiles of the ASGS solution (τ formulation given by Codina [10]) to the oil filtration problem on the coarse mesh. (a) Water saturation and (b) gas saturation.

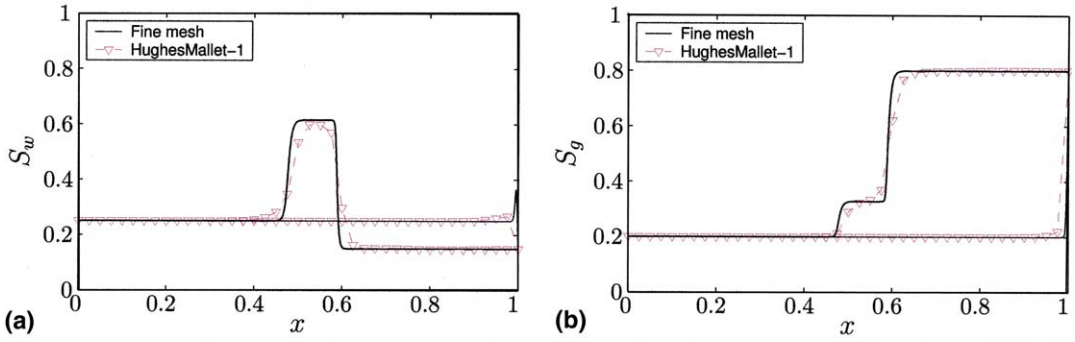

Fig. 6. Saturation profiles of the ASGS solution to the oil filtration problem. "Canonical form" of the shock-capturing diffusion. (a) Water saturation and (b) gas saturation.

In Fig. 6 we plot the results for the "canonical form" of the shock-capturing diffusion. It is found that this formulation is effective at eliminating the oscillatory behavior (compare with Fig. 4), but at the cost of being a bit too diffusive.

In Fig. 7 we plot the numerical solution obtained when the "global-gradient form" of the discontinuity-capturing diffusion is employed, with the following values of the parameters:

$$\boldsymbol{U}_{\mathrm{sc}} = (0.5, 0.5), \quad C_{\mathrm{sc}} = 2. \tag{64}$$

The latter method is able to remove the localized oscillatory behavior of the ASGS solution but is, for the parameters used, slightly too diffusive as well.

The reason for considering the novel expression of the shock-capturing diffusion as a viable alternative to existing formulations stems from the distribution of the numerical diffusion that is actually introduced by each method. In Fig. 8 and Fig. 9 we plot the profile of additional diffusion introduced by the "canonical form" and the "global-gradient form", respectively, at two different simulation times. While the existing formulation adds a significant amount of diffusion almost everywhere, the proposed formulation automatically introduces numerical dissipation *only* in the neighborhood of the sharp features of the solution. The latter is precisely the desired behavior of a discontinuity-capturing mechanism.

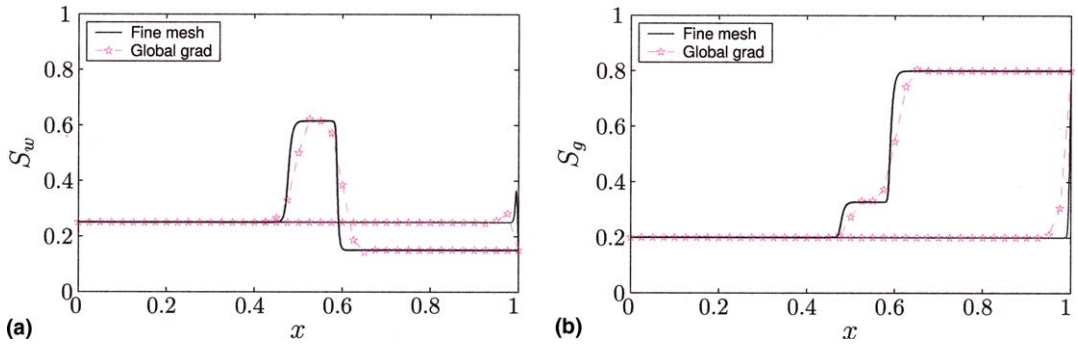

Fig. 7. Saturation profiles of the ASGS solution to the oil filtration problem. Proposed formulation of the shock-capturing diffusion. (a) Water saturation and (b) gas saturation.

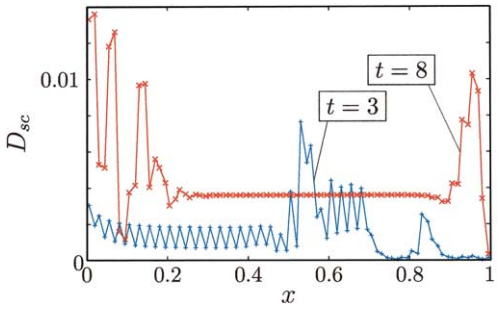

Fig. 8. Profiles of shock capturing diffusion introduced by the "canonical form" at two different times.

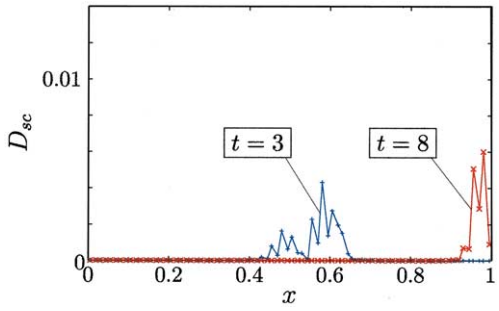

Fig. 9. Profiles of shock capturing diffusion introduced by the proposed formulation at two different times.

3.2.2. Water–gas injection in a reservoir

The second application involves simultaneous injection of water and gas into a porous medium filled with oil and gas, and a small amount of water. Initially, the medium has constant normalized saturations: $S_w = 0.05$,$S_g = 0.4$, and $S_o = 0.55$. Gas and water are injected in such proportion that the normalized water and gas saturations at the inlet are $S_w = 0.85$ and $S_g = 0.15$, respectively. The injected saturations are assumed to be constant throughout the experiment. The values of initial and injected saturations used in this

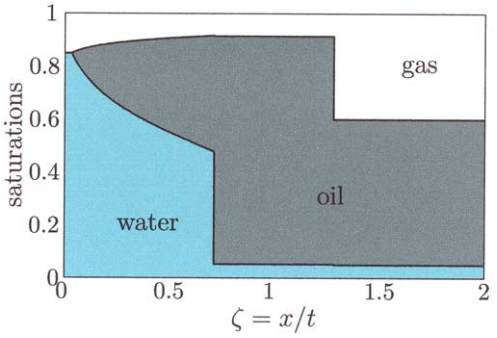

Fig. 10. Saturation profiles of the *exact solution* to the water–gas injection problem. Saturations of each phase are plotted against the similarity variable $\zeta = x/t$.

example are representative of a linear water-alternating-gas (WAG) injection process in a hydrocarbon reservoir after primary production.

Analytical solution. The analytical solution to the water–gas injection problem described above is a sequence of two waves, where the slow wave is a rarefaction-shock, and the fast wave is a single shock [32]. The fluid saturation profiles of the analytical solution are shown in Fig. 10. The profiles are plotted against the similarity variable $\zeta = x/t$. The slow wave involves mainly displacement of oil by injected water, and the fast wave corresponds to a displacement of gas by oil. An oil bank with higher oil saturations than those of the initial and injected states is formed.

"*Reference*" *numerical solution*. We compute a "reference" numerical solution to the water–gas injection problem with small capillary diffusion coefficients:

$$\epsilon_\omega = 0.001, \quad \epsilon_g = 0.002. \tag{65}$$

We use the standard Galerkin formulation on a very fine mesh of 4000 elements ($h = 2.5 \times 10^{-4}$), and a Crank–Nicolson time integration scheme with $\delta t = 5 \times 10^{-5}$. For this space and time discretization, the element Peclet and Courant numbers are, respectively:

$$Pe := \frac{\sigma_{\max} h}{\epsilon_{\min}} \approx 0.3, \tag{66}$$

$$Co := \frac{\sigma_{\max} \delta t}{h} \approx 0.25. \tag{67}$$

In Fig. 11 we plot the water and gas saturation profiles of the "reference" numerical solution at $t = 0.5$, together with the capillarity-free analytical solution. The numerical solution correctly captures the location and magnitude of the shocks, and provides an accurate representation of the rarefaction fan. Additional simulations with different space and time discretizations, and different capillary diffusion coefficients, confirm convergence of the standard Galerkin method to the entropy solution of the problem.

Standard Galerkin solution. The problem is solved with the same physical parameters on a much coarser mesh of 40 elements and a time step $\delta t = 0.005$. The element Peclet number is now $Pe \approx 30$, and the element Courant number remains $Co \approx 0.25$. The results are shown in Fig. 12 at two different simulation times ($t = 0.5$ and $t = 2$), and compared with the reference numerical solution. The Galerkin solution is completely oscillatory, especially after breakthrough of the water front.

Algebraic subgrid scale solutions. The numerical solution produced by the ASGS method with the τ formulation of Hughes and Mallet [23] is shown in Fig. 13. The behavior of the method is remarkable, considering that a very coarse mesh of only 40 elements was used. The stabilizing term is able to remove the

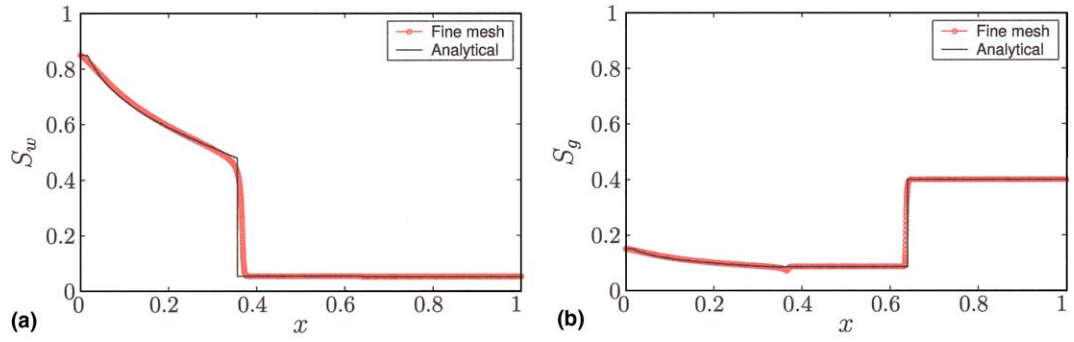

Fig. 11. Saturation profiles of the standard Galerkin solution to the water–gas injection problem on a fine mesh of 4000 elements, and comparison to the analytical solution of the capillarity-free case. Results are shown at time $t = 0.5$. (a) Water saturation and (b) gas saturation.

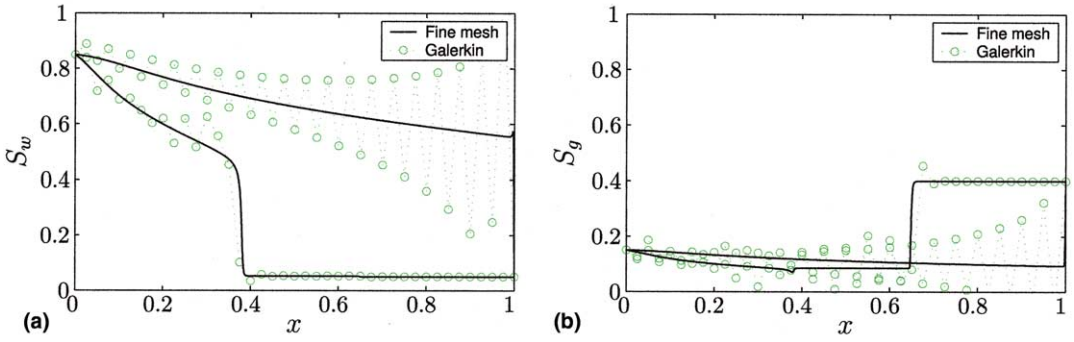

Fig. 12. Saturation profiles of the standard Galerkin solution to the water–gas injection problem on a coarse mesh of 40 elements. Results are shown at times $t = 0.5$ and $t = 2$. (a) Water saturation and (b) gas saturation.

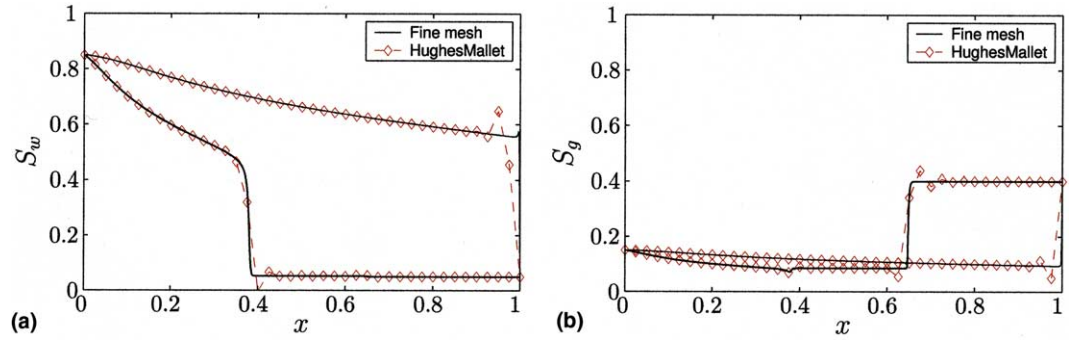

Fig. 13. Saturation profiles of the ASGS solution (τ formulation given by Hughes and Mallet [23]) to the water–gas injection problem on the coarse mesh. (a) Water saturation and (b) gas saturation.

global oscillatory behavior of the standard Galerkin method, while preserving a sharp definition of the shocks and boundary layers.

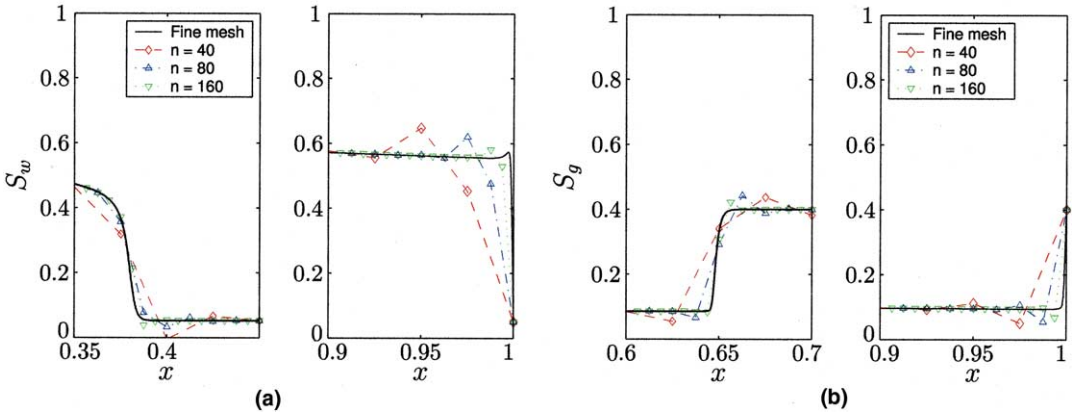

Fig. 14. Zoomed view of the saturation profiles of the ASGS solution, showing the behavior of the method as the mesh is refined. (a) Water saturation and (b) gas saturation.

It is important to investigate the behavior of the algebraic subgrid scale method as the mesh is refined. In Fig. 14 we show a zoomed view of the saturation profiles at two different times ($t = 0.5$ and $t = 2$), computed with three different grids of 40, 80, and 160 elements. The ASGS method is well-behaved, in the sense that the amplitude of the small over/undershoots decreases as the mesh is refined, and the solution does not suffer from Gibbs phenomena near the discontinuities. We illustrate this behavior quantitatively in Fig. 15, where we plot the evolution of the L^∞-norm of the error—the amplitude of the over/undershoot—as the grid is refined. The analysis indicates that, at least for this case, convergence in the L^∞-norm is super-linear.

Other formulations of the matrix $\boldsymbol{\tau}$ of stabilizing coefficients [10,40] do not yield results of the same quality as those of Fig. 13. In some cases the method even fails to converge, emphasizing the importance of an appropriate choice of $\boldsymbol{\tau}$ for each particular problem.

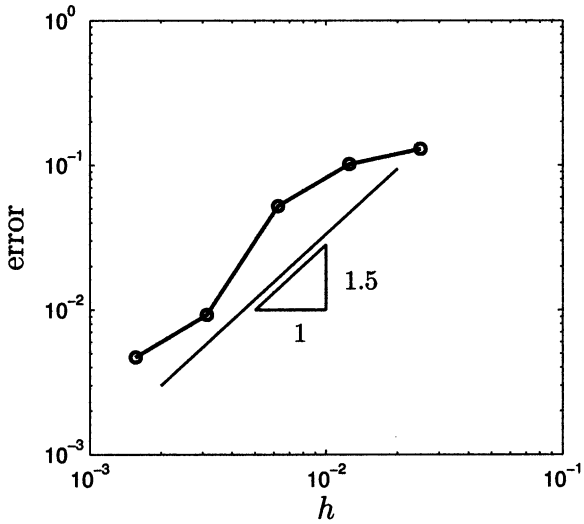

Fig. 15. Evolution of the L^∞-norm of the error (amplitude of the over/undershoot) at $t = 2$, as the mesh is refined.

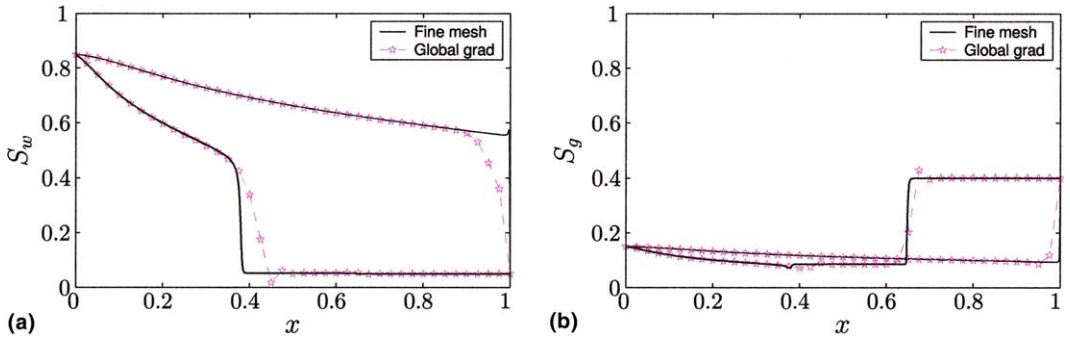

Fig. 16. Saturation profiles of the ASGS solution to the water–gas injection problem. Proposed formulation of shock-capturing diffusion. (a) Water saturation and (b) gas saturation.

Stabilized solutions with shock capturing diffusion. Despite the effective stabilization of the ASGS method with the matrix of stabilizing coefficients given by Hughes and Mallet [23], some local overshooting is still present in the solution. We make use of a discontinuity-capturing technique to remove the spurious wiggles. In Fig. 16 we plot the numerical solution obtained after using the ASGS method above in conjunction with the proposed "global-gradient form" of the shock-capturing diffusion. We use the following parameters:

$$\boldsymbol{U}_{\mathrm{sc}} = (0.5, 0.5), \quad C_{\mathrm{sc}} = 2. \tag{68}$$

The computed solution does not degrade the accuracy in the smooth regions—the rarefaction fan and the constant saturation states—while effectively enhancing stability near the sharp gradients.

The profile of additional diffusion introduced by the discontinuity-capturing term is plotted at simulation times $t = 0.5$ and $t = 2$ in Fig. 17. It is apparent that the amount of artificial diffusion is negligible everywhere, except in the vicinity of discontinuities. The "canonical form" of the shock-capturing diffusion described earlier is either less effective or even fails to converge.

It is also important to determine the sensitivity of the proposed shock-capturing operator to the choice of the coefficients involved in the formulation. In Fig. 18 we plot the solution for different values of the constant C_{sc}. As expected, the solution is more diffusive as the coefficient C_{sc} increases, and approaches the ASGS solution (Fig. 13) when C_{sc} tends to zero. We conclude that there is a fairly wide range of values of the constant for which the method yields a stable solution.

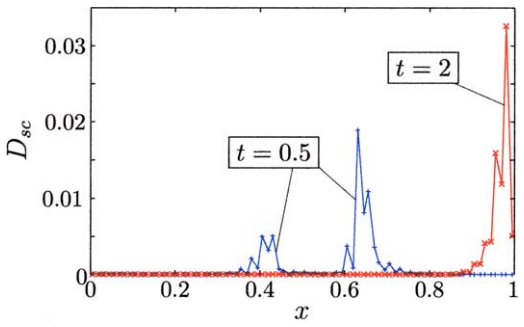

Fig. 17. Profiles of shock capturing diffusion introduced by the proposed formulation at two different times.

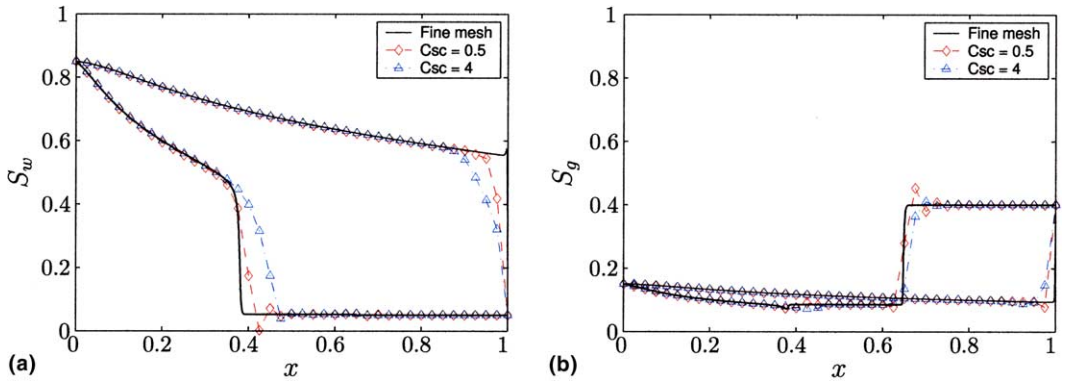

Fig. 18. Saturation profiles of the ASGS solution with the proposed formulation of shock-capturing diffusion for different values of the coefficient C_{sc}. (a) Water saturation and (b) gas saturation.

4. Shallow water equations

We apply the variational multiscale method to the one-dimensional shallow water equations in conservation variables. We show the performance of the method on a problem involving a wave reflection.

4.1. Mathematical formulation

We write the system of one-dimensional shallow water equations as follows (see, e.g., [35]):

$$\begin{aligned} \partial_t h + \partial_x m - v\partial_{xx} h &= 0, \\ \partial_t m + \partial_x \left(\frac{m^2}{h} + \frac{1}{2} g h^2 \right) - v\partial_{xx} m &= 0, \end{aligned} \tag{69}$$

where h is the water depth, m is the discharge, g is the gravitational acceleration, and v is a diffusion coefficient due to viscosity effects. The system (69) can be expressed in the standard form (1) by defining:

$$\boldsymbol{u} = \begin{pmatrix} h \\ m \end{pmatrix}, \quad \boldsymbol{f} = \begin{pmatrix} m \\ m^2/h + gh^2/2 \end{pmatrix}, \quad \mathbf{D} = \begin{pmatrix} v & 0 \\ 0 & v \end{pmatrix}. \tag{70}$$

The system of shallow water equations is strictly hyperbolic in the viscosity-free limit, as long as $h > 0$.

4.2. Representative numerical simulations

We solve the shallow water equations in the bounded domain $[0, L]$, with $L = 10$. The initial conditions are those of a quiescent water hump:

$$\begin{aligned} h(x,0) &= h_0(x), \\ m(x,0) &= 0, \end{aligned} \tag{71}$$

where the initial water profile is sketched in Fig. 19. The boundary conditions are of reflection type:

$$\begin{aligned} \partial_x h(0,t) = \partial_x h(L,t) &= 0, \\ m(0,t) = m(L,t) &= 0. \end{aligned} \tag{72}$$

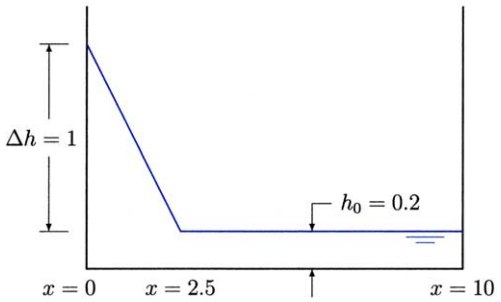

Fig. 19. Initial conditions employed in the numerical simulations of the shallow water equations.

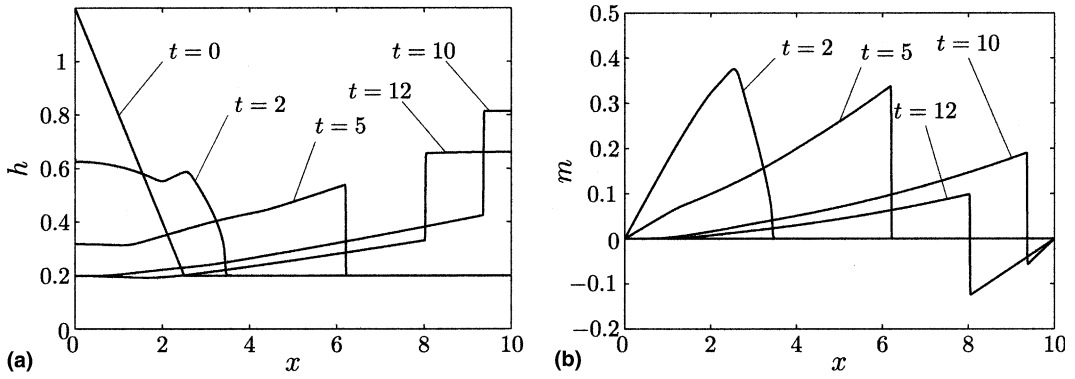

Fig. 20. Standard Galerkin solution to the shallow water equations on a fine mesh of 4000 elements. Reflection at the right boundary occurs at $t \approx 9$. (a) Water depth and (b) discharge.

In our numerical simulations, we take the gravitational acceleration $g = 1$, and a small value of the diffusion coefficient $\nu = 0.001$.

"*Reference*" *numerical solution*. We compute a "reference" numerical solution, using the standard Galerkin method on a very fine grid of 4000 elements ($h = 2.5 \times 10^{-3}$) and a Crank–Nicolson time stepping with $\delta t = 5 \times 10^{-4}$. The element Peclet and Courant numbers are

$$Pe := \frac{\sigma_{\max} h}{\nu} \approx 2.5, \tag{73}$$

$$Co := \frac{\sigma_{\max} \delta t}{h} \approx 0.2. \tag{74}$$

In Fig. 20 we plot the water depth and the discharge at various times. A shock forms after time $t = 2$, and the wave reflects at the right boundary at time $t \approx 9$. Additional numerical simulations with different space and time discretizations confirm convergence of the standard Galerkin method to the entropy solution of the problem.

Standard Galerkin solution. We solve the problem using the standard Galerkin method on a very coarse grid of 40 elements and time step $\delta t = 0.05$. The corresponding Peclet and Courant numbers are $Pe \approx 250$ and $Co \approx 0.2$, respectively. The results of the simulation are shown in Fig. 21, and compared with the reference numerical solution. The solution is polluted with global spurious oscillations. The lack of stability is especially severe after the wave reflection, and the method is unable to produce a solution after $t \approx 11$.

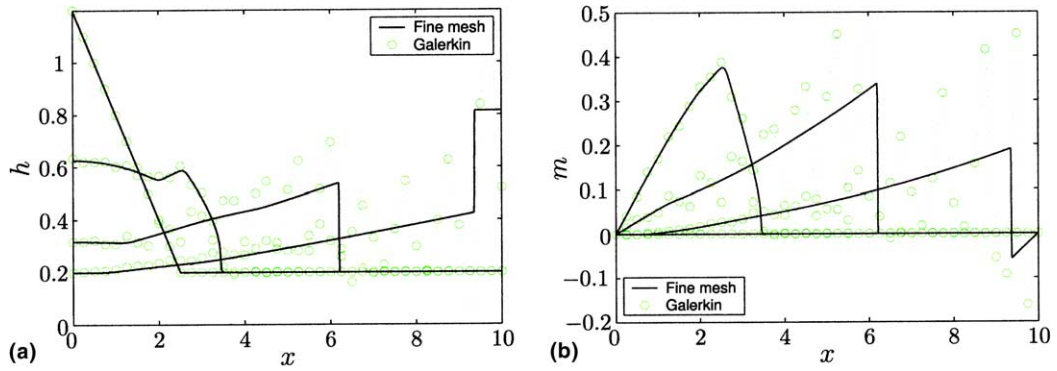

Fig. 21. Standard Galerkin solution to the shallow water equations on a coarse mesh of 40 elements. The method was unable to produce a solution at $t = 12$. (a) Water depth and (b) discharge.

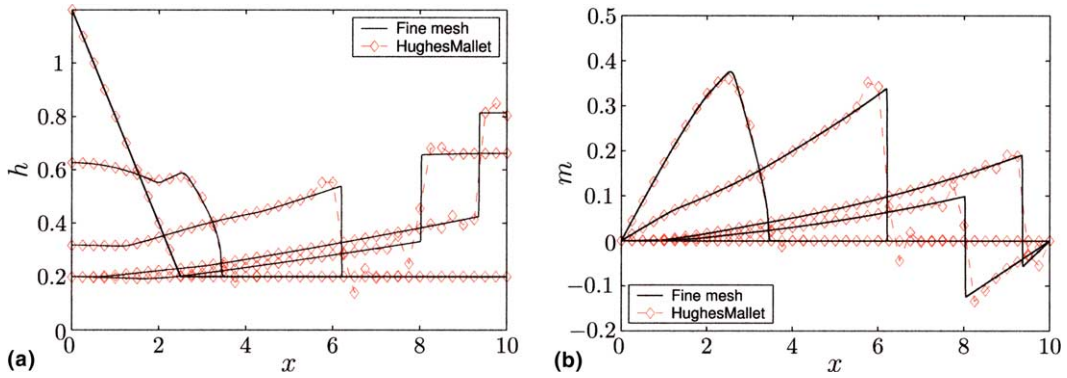

Fig. 22. ASGS solution (τ formulation given by Hughes and Mallet [23]) to the shallow water equations on a coarse mesh of 40 elements. Results are shown at times $t = 0$, 2, 5, 10 and 12. (a) Water depth and (b) discharge.

Algebraic subgrid scale solution. In Fig. 22 we show the numerical solution obtained with the ASGS method, using the same space and time discretization as before. The τ formulation of Hughes and Mallet [23] was used. The stabilizing effect of the subgrid-scale term is apparent: the solution does not display global spurious oscillations, and the method is perfectly stable after the wave reflection. Other formulations of the matrix τ, however, rendered numerical solutions of lower quality, or even prevented the method from converging.

Stabilized solution with shock-capturing diffusion. The ASGS solution is enhanced by incorporating a discontinuity-capturing technique. The results obtained with the "canonical" form of the shock-capturing diffusion are shown in Fig. 23. The method removes the localized wiggles of the ASGS solution near the fronts without introducing excessive smearing.

5. Conclusions

We have presented a fairly general formulation for the numerical solution of nonlinear systems of conservation laws, and applied it to the simulation of one-dimensional three-phase flow through porous media,

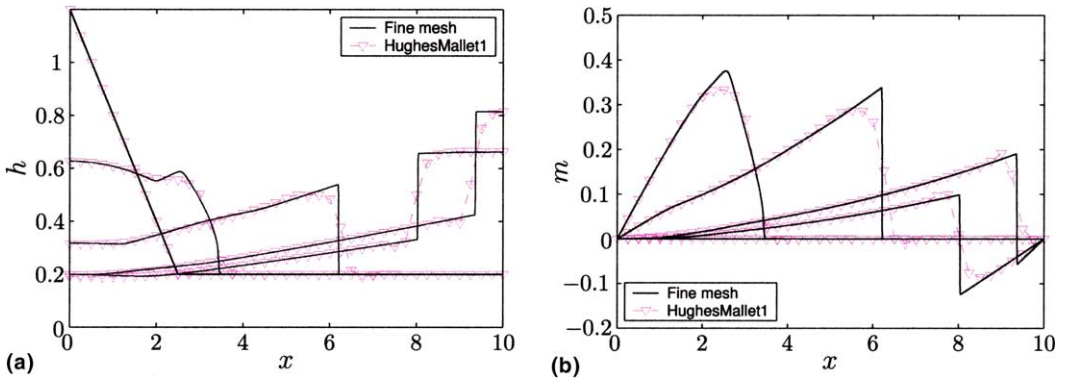

Fig. 23. ASGS solution with shock-capturing to the shallow water equations on a coarse mesh. (a) Water depth and (b) discharge.

and the one-dimensional shallow water equations. The method is based on the original framework presented in [21], and entails a multiple-scale decomposition of the solution into resolved and unresolved scales. The effect of the unresolved subgrid scales on the resolved grid scales introduces a stabilizing term in the formulation. Key distinctive features of the formulation developed herein are: (1) the multiscale split is performed *before* any linearization of the equations (which are kept in conservation form); (2) the multiscale solution is *not* reconstructed from point values of coarse-scale and subgrid-scale solutions; and (3) a novel shock-capturing technique is proposed to enhance stability of the solution in the neighborhood of fronts.

From the results presented in Sections 3 and 4, we conclude that the proposed stabilized method yields numerical solutions of very good quality to challenging, highly nonlinear, nearly hyperbolic problems. Solutions computed on very coarse grids display excellent stability and accuracy. The algebraic subgrid model employed is quite sensitive, however, to the choice of the matrix of stabilizing coefficients $\boldsymbol{\tau}$. The definition of $\boldsymbol{\tau}$ given by Hughes and Mallet [23], which requires the solution of an eigenvalue problem, seems to be the most applicable to the type of problems considered in this paper. The novel "global-gradient form" of the discontinuity-capturing diffusion provides an alternative to existing formulations. The numerical simulations show that, in contrast to the canonical expression, the numerical diffusion introduced by the proposed formulation is confined to the vicinity of discontinuities in the solution.

Several issues deserve further investigation. One of the topics that is currently being addressed is the study of a different approximation to the subscales. In particular, we are interested in a *numerical* approximation of the subgrid scale problem with appropriate basis functions—high-order finite elements, wavelets, etc., which are potentially capable of capturing the sharp features of the solution that the coarse mesh is unable to resolve. Extension of the formulation to multidimensional problems is presented in a forthcoming paper.

Acknowledgements

The authors would like to thank Prof. Ramon Codina for reviewing an earlier version of the manuscript, and offering many constructive suggestions. This work was supported in part by the US Department of Energy under Contract No. DE-AC03-76SF00098. Funding provided by Barrié de la Maza, Jane Lewis, and Repsol-YPF fellowships, awarded to the first author, is also gratefully acknowledged.

References

[1] T. Arbogast, Numerical subgrid upscaling of two-phase flow in porous media, in: Z. Chen, R.E. Ewing, Z.-C. Shi (Eds.), Numerical Treatment of Multiphase Flow in Porous Media, Lecture Notes in Physics, vol. 552, Berlin, Springer, 2000, pp. 35–49.
[2] T. Arbogast, Implementation of a locally conservative numerical subgrid upscaling scheme for two-phase Darcy flow, Comput. Geosci. 6 (3–4) (2002) 453–481.
[3] K. Aziz, A. Settari, Petroleum Reservoir Simulation, Elsevier, London, 1979.
[4] C. Baiocchi, F. Brezzi, L.P. Franca, Virtual bubbles and Galerkin/least-squares type methods (Ga.L.S), Comput. Methods Appl. Mech. Engrg. 105 (1993) 125–141.
[5] F. Brezzi, L.P. Franca, T.J.R. Hughes, A. Russo, $b = \int g$, Comput. Methods Appl. Mech. Engrg. 145 (1997) 329–339.
[6] A.N. Brooks, T.J.R. Hughes, Streamline upwind Petrov–Galerkin formulations for convection dominated flows with particular emphasis on the incompressible Navier–Stokes equations, Comput. Methods Appl. Mech. Engrg. 32 (1982) 199–259.
[7] G. Chavent, J. Jaffré, Mathematical Models and Finite Elements for Reservoir Simulation, Studies in Mathematics and its Applications, vol. 17, Elsevier, North-Holland, 1986.
[8] R. Codina, A discontinuity-capturing crosswind-dissipation for the finite element solution of the convection-diffusion equation, Comput. Methods Appl. Mech. Engrg. 110 (1993) 325–342.
[9] R. Codina, Comparison of some finite element methods for solving the diffusion–convection–reaction equation, Comput. Methods Appl. Mech. Engrg. 156 (1998) 185–210.
[10] R. Codina, On stabilized finite element methods for linear systems of convection–diffusion–reaction equations, Comput. Methods Appl. Mech. Engrg. 188 (2000) 61–82.
[11] R. Codina, A stabilized finite element method for generalized stationary incompressible flows, Comput. Methods Appl. Mech. Engrg. 190 (2001) 2681–2706.
[12] R. Codina, Stabilized finite element approximation of transient incompressible flows using orthogonal subscales, Comput. Methods Appl. Mech. Engrg. 191 (39–40) (2002) 4295–4321.
[13] R. Codina, J. Blasco, Analysis of a stabilized finite element approximation of the transient convection–diffusion–reaction equation using orthogonal subscales, Comput. Visual. Sci. 4 (3) (2002) 167–174.
[14] L.P. Franca, A. Nesliturk, M. Stynes, On the stability of residual free bubbles for convection–diffusion problems and their approximation by a two-level finite element method, Comput. Methods Appl. Mech. Engrg. 166 (1998) 35–49.
[15] A.C. Galeão, E.G. Dutra do Carmo, A consistent approximate upwind Petrov–Galerkin method for convection-dominated problems, Comput. Methods Appl. Mech. Engrg. 68 (1988) 83–95.
[16] K. Garikipati, T.J.R. Hughes, A study of strain localization in a multiple scale framework—the one-dimensional problem, Comput. Methods Appl. Mech. Engrg. 159 (1998) 193–222.
[17] K. Garikipati, T.J.R. Hughes, A variational multiscale approach to strain localization—formulation for multidimensional problems, Comput. Methods Appl. Mech. Engrg. 188 (2000) 39–60.
[18] G. Hauke, A simple subgrid scale stabilized method for the advection–diffusion–reaction equation, Comput. Methods Appl. Mech. Engrg. 191 (2002) 2925–2947.
[19] G. Hauke, A. García-Olivares, Variational subgrid scale formulations for the advection–diffusion–reaction equation, Comput. Methods Appl. Mech. Engrg. 190 (2001) 6847–6865.
[20] T.Y. Hou, X.-H. Wu, A multiscale finite element method for elliptic problems in composite materials and porous media, J. Comput. Phys. 134 (1997) 169–189.
[21] T.J.R. Hughes, Multiscale phenomena: Green's functions, the Dirichlet-to-Neumann formulation, subgrid scale models, bubbles and the origins of stabilized methods, Comput. Methods Appl. Mech. Engrg. 127 (1995) 387–401.
[22] T.J.R. Hughes, G.R. Feijóo, L. Mazzei, J.-B. Quincy, The variational multiscale method—a paradigm for computational mechanics, Comput. Methods Appl. Mech. Engrg. 166 (1998) 3–24.
[23] T.J.R. Hughes, M. Mallet, A new finite element formulation for computational fluid dynamics: III. The generalized streamline operator for multidimensional advective–diffusive systems, Comput. Methods Appl. Mech. Engrg. 58 (1986) 305–328.
[24] T.J.R. Hughes, M. Mallet, A new finite element formulation for computational fluid dynamics: IV. A discontinuity-capturing operator for multidimensional advective–diffusive systems, Comput. Methods Appl. Mech. Engrg. 58 (1986) 329–336.
[25] T.J.R. Hughes, M. Mallet, A. Mizukami, A new finite element formulation for computational fluid dynamics: II. Beyond SUPG, Comput. Methods Appl. Mech. Engrg. 54 (1986) 341–355.
[26] T.J.R. Hughes, L. Mazzei, K.E. Jansen, Large Eddy Simulation and the variational multiscale method, Comput. Visual. Sci. 3 (2000) 47–59.
[27] T.J.R. Hughes, L. Mazzei, A.A. Oberai, The multiscale formulation of large eddy simulation: decay of homogeneous isotropic turbulence, Phys. Fluids 13 (2) (2001) 505–512.
[28] T.J.R. Hughes, A.A. Oberai, L. Mazzei, Large eddy simulation of turbulent channel flows by the variational multiscale method, Phys. Fluids 13 (6) (2001) 1784–1799.

[29] K.E. Jansen, S.S. Collis, C. Whiting, F. Shakib, A better consistency for low-order stabilized finite element methods, Comput. Methods Appl. Mech. Engrg. 174 (1999) 153–170.
[30] R. Juanes, Displacement theory and multiscale numerical modeling of three- phase flow in porous media, Ph.D. Dissertation, University of California at Berkeley, March 2003.
[31] R. Juanes, T.W. Patzek, Multiple scale stabilized finite elements for the simulation of tracer injections and waterflood, in: SPE/DOE Thirteenth Symposium on Improved Oil Recovery, Tulsa, OK, April 13–17, 2002 (SPE 75231), submitted to Soc. Pet. Eng. J.
[32] R. Juanes, T.W. Patzek, Analytical solution to the Riemann problem of three-phase flow in porous media, Transp. Porous Media 55 (1) (2004) 47–70.
[33] R. Juanes, T.W. Patzek, Multiscale-stabilized finite element methods for miscible and immiscible flow in porous media, J. Hydraul. Res. 42 (special issue) (2004) 131–140.
[34] R. Juanes, T.W. Patzek, Relative permeabilities for strictly hyperbolic models of three-phase flow in porous media, Transp. Porous Media 57 (2) (2004) 125–152.
[35] R.J. LeVeque, Finite Volume Methods for Hyperbolic ProblemsCambridge Texts in Applied Mathematics, Cambridge University Press, 2002.
[36] A. Masud, T.J.R. Hughes, A stabilized mixed finite element method for Darcy flow, Comput. Methods Appl. Mech. Engrg. 191 (39–40) (2002) 4341–4370.
[37] A.A. Oberai, P.M. Pinsky, A multiscale finite element method for the Helmholtz equation, Comput. Methods Appl. Mech. Engrg. 154 (1998) 281–297.
[38] A.A. Oberai, P.M. Pinsky, A residual-based finite element method for the Helmholtz equation, Int. J. Numer. Meth. Engrg. 49 (3) (2000) 399–419.
[39] M. Peszynska, M.F. Wheeler, I. Yotov, Mortar upscaling for multiphase flow in porous media, Comput. Geosci. 6 (1) (2002) 73–100.
[40] F. Shakib, T.J.R. Hughes, Z. Johan, A new finite element formulation for computational fluid dynamics: X. The compressible Euler and Navier–Stokes equations, Comput. Methods Appl. Mech. Engrg. 89 (1991) 141–219.
[41] V. Thomée, Galerkin Finite Element Methods for Parabolic Problems, Springer Series in Computational Mathematics, vol. 25, Springer-Verlag, Berlin, 1997.